



HAL
open science

UV Emission from GaN Wires with m -Plane Core–Shell GaN/AlGaN Multiple Quantum Wells

Vincent Grenier, Sylvain Finot, Gwenolé Jacopin, Catherine Bougerol, Nicolas Mollard, Bruno Gayral, Eva Monroy, J. Eymery, Christophe Durand

► **To cite this version:**

Vincent Grenier, Sylvain Finot, Gwenolé Jacopin, Catherine Bougerol, Nicolas Mollard, et al.. UV Emission from GaN Wires with m -Plane Core–Shell GaN/AlGaN Multiple Quantum Wells. *ACS Applied Materials & Interfaces*, 2020, 12 (39), pp.44007-44016. 10.1021/acsami.0c08765 . cea-02963131

HAL Id: cea-02963131

<https://cea.hal.science/cea-02963131>

Submitted on 18 Dec 2020

HAL is a multi-disciplinary open access archive for the deposit and dissemination of scientific research documents, whether they are published or not. The documents may come from teaching and research institutions in France or abroad, or from public or private research centers.

L'archive ouverte pluridisciplinaire **HAL**, est destinée au dépôt et à la diffusion de documents scientifiques de niveau recherche, publiés ou non, émanant des établissements d'enseignement et de recherche français ou étrangers, des laboratoires publics ou privés.

UV-emission from GaN wires with *m*-plane core-shell GaN/AlGaN multiple quantum wells

Vincent Grenier*, Sylvain Finot, Gwénolé Jacopin, Catherine Bougerol, Nicolas Mollard, Bruno Gayral, Eva Monroy, Joël Eymery and Christophe Durand*

ABSTRACT:

The present work reports high quality non-polar GaN/Al_{0.6}Ga_{0.4}N multiple quantum wells (MQWs) grown in core-shell geometry by metalorganic vapor phase epitaxy on the *m*-plane sidewalls of \bar{c} -oriented hexagonal GaN wires. Optical and structural studies reveal UV emission originating from the core-shell GaN/AlGaN MQWs. Tuning the *m*-plane GaN QW thickness from 4.3 to 0.7 nm leads to a shift of the emission from 347 to 292 nm, consistent with Schrödinger-Poisson calculations. The evolution of the luminescence with temperature displays signs of strong localization, especially for samples with thinner GaN QWs and no evidence of quantum confinement Stark effect, as expected for non-polar *m*-plane surfaces. The internal quantum efficiency derived from the photoluminescence intensity ratio at low and room temperature is maximum (~7.3 %) for 2.6 nm-thick quantum wells, emitting at 325 nm and shows a large drop for thicker QWs. An extensive study of the PL quenching with temperature is presented. Two non-radiative recombination paths are activated at different temperatures. The low temperature path is found to be intrinsic to the heterostructure, whereas the process that dominates at high temperature depends on the QW thickness and is strongly enhanced for QWs larger than 2.6 nm, causing a drop of the internal quantum efficiency.

KEYWORDS: *Wires, UV, MOVPE, GaN/AlGaN heterostructures, nonpolar planes*

■ INTRODUCTION

Ultraviolet (UV) light emitting diodes (LEDs) have recently emerged to replace traditional mercury lamps due to their significant advantages, such as long lifetime, fast switching, compactness and wavelength tuning. LEDs emitting UV-C light are highly demanded for bactericide applications (water and surface sterilization).¹ Compared to standard blue LEDs, which display extremely high external quantum efficiency (EQE > 80%), commercial UV LEDs exhibit relatively low EQE values (EQE ≤ 20% for UV-A and UV-B and ≤ 1% for UV-C).²

A typical UV LED consists of a *c*-oriented AlGa_xN p-n junction including Al_xGa_{1-x}N/Al_yGa_{1-y}N multiple quantum wells (MQWs) in the depletion region. The use of AlGa_xN nanowires has been proposed as path to improve the UV light emission efficiency beyond that of planar devices thanks to the lower density of extended defects, enhanced light extraction efficiency and the high p-type doping levels attained in nanowire-shaped Al-rich AlGa_xN materials.³⁻⁶ For instance, >2.6 times improvement of the EQE has been demonstrated for top-down etched nanowires in comparison to the same wafer processed with planar geometry.⁷ Most of the research efforts on nanowires for UV emission refer to structures synthesized by molecular beam epitaxy (MBE). The directionality of the MBE technique allows growing complex axial heterostructures.^{8,9} On the contrary, very few studies related to UV emission are based on wires grown by metal-organic vapor phase epitaxy (MOVPE)¹⁰⁻¹⁷ technique, which is the most implanted industrial method for LED fabrication. The gas-phase transport mechanism of MOVPE growth allows synthesizing core-shell heterostructures, since all the wire surfaces (top and sidewalls) are exposed to chemical reactants. Core-shell quantum wells (QWs) on non-polar *m*-plane {10 $\bar{1}$ 0} wire sidewalls do not present quantum confined Stark effect

(QCSE). Therefore, the QW emission is blue shifted and the radiative lifetime is shorter than in polar c -plane structures with the same QW width. Core-shell systems have been intensively studied in the case of InGaN/GaN MQWs for the development of wire-based LEDs in the blue-green spectral range.¹⁸⁻²⁰

Focusing on wires for UV emission grown by MOVPE, we can distinguish core-shell structures with three types of inner core: AlN¹⁰⁻¹², Al_xGa_{1-x}N ($x < 0.35$)^{13,14} and GaN¹⁵⁻¹⁷. Wires with AlN core and core-shell AlGaN/AlN QWs emitting at 260 nm exhibit a 40-times enhancement of the photoluminescence (PL) intensity with respect to planar structures.²¹ The same core-shell structures with AlN core emitting at 229 nm have also been demonstrated.¹¹ However, no electroluminescence (EL) has been reported so far, due to the difficult electrical injection through the AlN inner core. On the contrary, wires with GaN core allow efficient carrier transport and EL from core-shell AlGaN-based heterostructures has already been reported: emission at 365 nm has been observed in core-shell n-i-p AlGaN heterostructures¹⁶ and peak emission at 318 nm has been attained with core-shell AlGaN/AlGaN MQWs grown around a GaN core.¹⁷ These studies represented the first demonstrations of UV-LEDs based on wires grown by MOVPE, but tuning the emission down to the UV-A range with core-shell GaN wires remains challenging using the MOVPE approach. A first difficulty is to limit the UV absorption in the GaN core, but GaN can be eliminated by *in situ* etching with an H₂/NH₃ gas mixture.²² Then, a main challenge stems from the large lattice mismatch between GaN and AlN (3.5% along c and 2.5% along a), which limits the studies to low Al-content AlGaN wells^{16,17} or thin GaN wells¹⁵ pseudomorphically grown on inner core wire. Further research on core-shell GaN MQWs is required in order to shift the emission towards shorter wavelengths while restraining defect formation.

In this context, this work is a systematic study of the UV light emission originating from core-shell *m*-plane GaN/AlGaIn MQWs grown by MOVPE on GaN wires as a function of the well thickness. UV emission in the range of 347-292 nm is achieved by tuning the QW thickness from 4.3 to 0.7 nm.

■ MATERIAL GROWTH

The growth of self-assembled GaN microwires is carried out in a 3 x 2" MOVPE close-coupled showerhead reactor on *c*-sapphire substrates. The growth process starts by annealing the substrate at 1050°C under NH₃ to prepare the sapphire surface with Al-termination, which favors the growth of GaN with N-polarity. Then, a thin SiN_x layer is formed by injecting simultaneously silane (SiH₄) and NH₃. Then, we inject trimethylgallium (TMGa) (135 μmol.min⁻¹) and NH₃ (2.232 mmol.min⁻¹) diluted in N₂ carrier gas flow (8000 sccm) at 1040°C and 800 mbar using a very low V/III ratio (~50), to nucleate GaN seeds. After 10 s, we add a high silane flux (~200 nmol.min⁻¹) to start the wire growth exhibiting mainly the N-polarity.²³ Under these conditions, the presence of silane spontaneously forms a thin SiN_x passivation layer on the *m*-plane sidewalls of the GaN wires, which favors the vertical growth. On the other hand, such a high flux of silane results in heavily n⁺⁺-doped GaN (N_d ~ 10²⁰ cm⁻³), which facilitates current injection.²⁴ The silane is switched off after 300 s, and the growth of GaN continues for another 400 s. During this step, the remaining silane concentration in the reactor results in residual n⁺ doped GaN wires (N_d ~ 10¹⁹ cm⁻³).²⁵ The two different doped regions (n⁺⁺ and n⁺-GaN) will be referred to as bottom and top parts of the wire, respectively. Then, a 50 nm-thick GaN epitaxial lateral shell (named "GaN spacer" hereafter) is grown at a substrate temperature of 900°C and a pressure of 150 mbar, using NH₃ and TMG fluxes

of 1500 sccm and 11 sccm, respectively, to get a V/III ratio around 2700. This GaN spacer allows burying the surface defects of the wire top part induced by the formation of an ultra-thin $\text{Si}_x\text{Ga}_y\text{N}$ residual layer.^{26,27} The same substrate temperature (900 °C) is kept during the growth of the barriers and QWs, but the growth pressure is decreased to 100 mbar to prevent pre-reaction of trimethylaluminium (TMAI) in the gas phase. Moreover, the gallium source is changed to triethylgallium (TEGa) to reduce drastically the growth rate of the QWs. Ten GaN/AlGaN QWs are grown on the *m*-plane wire sidewalls using a constant flow of TEG set at 25 sccm and adding a TMAI flux of 30 sccm for the barriers, which implies much higher V/III ratios (9000 and 6000 for QWs and barriers, respectively). In this work, the QW growth time is varied (200, 150, 120, 100, 80, 65, 50 and 30 s) to obtain different QW thickness, whereas the barrier growth time is maintained constant (76 s). To encapsulate the last AlGaN layer, a thin GaN cap of 1.5-2.5 nm is grown using the same conditions as for the GaN spacer.

■ RESULTS AND DISCUSSION

Figure 1a shows a 30°-tilted scanning electron microscopy (SEM) image of typical as-grown samples containing self-assembled microwires epitaxially grown on *c*-sapphire substrates. The estimated density is $\sim 10^7 \text{ cm}^{-2}$. The wires exhibit non-regular hexagonal cross section, they present six *m*-plane sidewall facets and a mainly flat \bar{c} -plane top surface, which is characteristic of wires grown along the N-polar direction.²⁸ Figure 1b shows an SEM image of a typical single wire mechanically dispersed on a silicon substrate. The wire length and diameter are typically in the range of 15-20 μm and 0.8-3 μm , respectively. A smooth shell covers only the top part of the wire, since SiN_x passivation of sidewalls limits the lateral growth around the bottom part.²⁹⁻³¹ This is

illustrated in the scheme in [Figure 1c](#), where the MQW shell growth occurs selectively only around the n⁺-doped top part, but a small shell (generally rough and with low crystal quality) is also present in the wire bottom part due to the low selectivity of the AlGa_N growth on SiN_x (see [Figure S1](#) for details). The structural characterization of the MQWs is performed on a transmission electron microscope operated at 200 kV, in either transmission (TEM) or HAADF-STEM (High Angle Annular Dark Field- Scanning Transmission) mode to enhance the chemical contrast (Z contrast) with a rather large camera length to be sensitive to the structural defects. Longitudinal cross-sections are prepared by focused Ga-ion beam (FIB) to get ~150 nm-thick slices. Two samples have been prepared and observed in this way: a first structure containing thick QWs (growth time 200 s) shown in [Figures 2a,b,c](#) and a second sample with intermediate QW thickness (growth time 120 s) shown in [Figures 2d,e,f](#). In the STEM-HAADF mode, the GaN core, spacer and QWs appear with bright contrast and the AlGa_N barriers are darker because of the smaller atomic number of Al with respect to Ga. The STEM images with low magnification ([Figures 2a,d](#)) show the high uniformity of core-shell GaN/AlGa_N heterostructures along the wire sidewalls and evidence a low density of extended defects. [Figures 2b,e](#) present the top part of the wires with intermediate magnification showing the N-polar MQWs on the top flat \bar{c} -plane surface and semi-polar MQWs on inclined facets at the top edges of the wire. [Figures 2c,f](#) correspond to high-resolution TEM (HRTEM) off-axis images with a 10° tilt around $[10\bar{1}0]$ direction from the $[11\bar{2}0]$ zone axis. From these images, the measured barrier thickness is 5.5 ± 1.5 nm for a growth time of 76 s, and QW thicknesses of 2.5 ± 0.5 and 4.4 ± 2.4 nm correspond to growth times of 120 and 200 s, respectively. Therefore, the QW and barrier growth rates are $V_{\text{QW}} = 1.3 \pm 0.5$ nm.min⁻¹ and $V_{\text{barrier}} = 4.3 \pm 1.2$ nm.min⁻¹. Note that the QW interfaces are sharper and symmetric compared to the core-shell InGa_N/Ga_N MQWs grown by

MOVPE.¹⁸ The error bar of the QW thickness comes mainly from QW-to-QW thickness variation. Especially, a variation as high as 50% is observed for the thicker QW sample (Figure S1). However, no significant fluctuation of the MQW thickness is observed along the wire sidewalls for both samples at the observation scale of Figures 2b,e. Considering this lateral growth rate, a linear interpolation is used to determine the GaN QW thicknesses of the sample series, obtaining 4.3, 3.3, 2.6, 2.2, 1.7, 1.4, 1.1, and 0.7 nm for the various QW growth times.

Cathodoluminescence (CL) measurements are performed in order to investigate the origin of the optical emission. Wires are dispersed on silicon substrates to prevent light emission from any residual planar growth. Figures 3a,c present SEM images on typical wires with 4.3 and 2.6 nm-thick QWs and Figures 3b,d their CL spectra as a function of the wire length (left panel) and their CL intensity map (right panel), both recorded at low temperature (5 K) with 5 kV acceleration voltage and 1 nA current. Looking at the spectra, it presents two lines, one peaking around 3.5 eV, which is assigned to GaN, and the other one at higher energy. This high-energy UV emission, assigned to transitions in the MQWs, is only detected at the top part of the wires. This result is consistent with the higher structural quality of the top part of the wire observed in Figure 2 with respect to the bottom part (Figure S1). Therefore, UV light is mostly coming from the MQWs forming the shell, *i.e.* from the *m*-plane wire sidewalls and not from the polar and semi-polar top surfaces. The CL map along the wire (intensity integrated over the full width at half maximum (FWHM) of the UV emission) shows that the UV emission for the sample with 2.6 nm QWs is blue shifted by 100 meV with respect to that from 4.3 nm QWs. In addition, a more pronounced shift (600 meV) is observed for the 0.7 nm-thick QWs emitting at 4.2 eV (Figure S4) consistent with an emission from core-shell QWs.

PL experiments on dispersed wires are carried out using a continuous-wave frequency-doubled solid-state laser (244 nm wavelength, 200 μ W excitation power, \approx 50 μ m spot diameter). [Figure 4a](#) presents the normalized PL spectra at 10 K for samples with QW thickness varying from 4.3 to 0.7 nm. The reduction of the QW thickness leads to a significant blue shift due to the stronger quantum confinement. UV emission down to 292 nm is thereby obtained for the thinnest QWs (0.7 nm). Another result of the reduction of the QW thickness is the increase of the PL FWHM from 90 meV for 4.3 nm-thick QWs to 393 meV for 0.7 nm-thick QWs. This broadening of the emission can be attributed to several effects including QW thickness fluctuations, interface roughness and short-range alloy inhomogeneity in the barriers.

[Figure 4b](#) shows the PL emission energy as a function of the QW thickness extracted from the PL data of [Figure 4a](#), where the error bars correspond to the distribution of 3-5 measurements acquired at different positions. This curve is consistent with the absence of QCSE in non-polar *m*-plane MQWs, since the increase of the QW thickness leads to a monotonous decrease of the energy that reaches the asymptotical value of the expected in bulk GaN band gap at 10 K emission (3.53 eV) as it was previously reported in GaN/AlGa_N³² and GaN/InAlN MQWs¹⁵. In this figure, the experimental data (red dots) are compared with calculations (colored lines plus symbols) performed with the nextnano³ software³³ using the 8-band **k,p** Schrödinger-Poisson method based on the material parameters in the Ref. [34](#). Lattice parameters and elastic coefficients of ternary alloys are extracted from those of binary compounds by linear interpolation. We modeled 5 periods of GaN/Al_{0.6}Ga_{0.4}N MQWs with 5.5-nm-thick barriers following a one-dimensional approximation. The Al content equal to 0.6 in the barriers provides the best agreement with experimental data. In terms of strain, three cases are considered. We calculate the emission for a pseudomorphic growth on GaN (i.e. Al_{0.6}Ga_{0.4}N is fully

strained, blue line plus symbols) and on $\text{Al}_{0.6}\text{Ga}_{0.4}\text{N}$ (i.e. GaN fully strained, dark line plus symbols). Then, to mimic a strain-balanced configuration, a calculation is performed assuming that the MQW system presents the in-plane lattice parameters of an $\text{Al}_{\bar{x}}\text{Ga}_{(1-\bar{x})}\text{N}$ ternary alloy with the average Al composition of the MQW period, \bar{x} . Note that the increase of the QW thickness from 0.7 to 4.3 nm decreases the value of \bar{x} from 0.53 to 0.33 and therefore the associated strain. These different calculations follow well the general trends of the experimental data and suggest a different relaxation state of GaN for large QW thicknesses.

A further analysis of the calculations can shine some light on the origin of the emission broadening. [Figure S2](#) compares the FWHM and the energy difference in the band-to-band e_1-h_1 transition caused by a thickness variation of $\pm 30\%$ and $\pm 40\%$ with respect to the nominal value (this QW-to-QW thickness variation is observed in [Figures 2b,e](#) and [Figure S1](#)). This comparison demonstrates that thickness fluctuations might be the dominant factor that explains the variation of the FWHM.

Light emission efficiency and non-radiative phenomena are studied by measuring the evolution of the PL as a function of temperature, using the previously described setup. [Figures 5a,b](#) depict the variation of the PL intensity with temperature for the two samples with 4.3 and 2.6 nm-thick QWs. As already described in the case of CL ([Figure 3](#)), the low-temperature spectra show two main contributions, namely a peak at 3.53 eV assigned to near band edge emission (NBE) from the Si-doped GaN core and an intense UV peak at higher energy from the non-polar m -plane QWs. As expected by the Moss-Burstein effect in heavily Si-doped GaN,³⁵ the GaN NBE is blue shifted with respect to the donor-bound exciton in non-intentionally doped bulk GaN (3.472-3.475 eV).^{36,37} The energy location of the observed NBE emission is consistent with doping levels in the range of 10^{19} - 10^{20} cm^{-3} .³⁸ As observed in [Figure 4a](#), the MQW luminescence at low

temperature is centered at 3.57 eV for 4.3-nm-thick GaN QWs (Figure 5a) and at 3.77 eV for 2.6-nm-thick GaN QWs (Figure 5b).

The variation of PL peak energy of the MQW emission as a function of temperature is shown in the inset of Figures 5a,b. It displays the typical S-shape that is usually attributed to carrier localization.³⁹⁻⁴¹ An estimation of the localization energy at low temperature can be deduced from the difference between the experimental data and the expected location of the emission at low temperature $E(T=0K)$ following the Varshni's law:

$$E(T) = E(0) + \frac{\alpha T^2}{\beta + T} \quad (1)$$

where $E(T)$ is the theoretical evolution of the transition energy as a function of temperature, and $\alpha = 0.59 \text{ meV.K}^{-1}$ and $\beta = 600 \text{ K}$ are two empirical constants.⁴² As shown in the inset of Figures 5a,b, the mean localization energies are equal to 16 ± 5 and $34 \pm 2 \text{ meV}$ for the 4.3 and 2.6 nm-thick GaN QWs, respectively. Larger localization energy is obtained for the 2.6 nm-thick QWs, as expected from the fact that a variation of thickness induces larger energy shifts in thinner QWs. For QWs $< 2.6 \text{ nm}$, a higher localization effect is also expected, but the value of the localization energy is difficult to extract from temperature-dependent measurements, since the deviations from Varshni equation are much more significant, as shown in Figure S3. This localization phenomena could explain emission inhomogeneity observed in low-temperature (5 K) CL maps (Figures 3 b,d). Interestingly, an additional signature of carrier localization is observed in local CL measurements for the 0.7 nm-thick QW sample, which exhibit sharp CL lines in the MQW spectra (Figure S4).

Figures 5c,d show the evolution of the normalized PL intensity $I(T)$ as a function of the inverse of the temperature in Arrhenius plots for the 4.3 and 2.6 nm-thick GaN QW

samples (blue dots). The trend does not follow a mono-exponential decay that would be expected in the case of a single thermally activated non-radiative path. Assuming two non-radiative processes, $I(T)$ can be described by a bi-exponential decay function⁴³:

$$I(T) = I_0 / \left[1 + a \exp\left(-\frac{E_a}{k_B T}\right) + b \exp\left(-\frac{E_b}{k_B T}\right) \right] = I_0 / (1 + P_a + P_b) \quad (2)$$

Where I_0 is the maximum intensity at low temperature, a and b are weighting factors that apply to each non-radiative recombination path, E_a and E_b are the related activation energies, and k_B is the Boltzmann constant. P_a and P_b represent the exponential decay of the two different non-radiative recombination paths. The extraction of the two energies (E_a and E_b) is performed using a three-step procedure described in the Supplementary Information (Figures S5-S9). This method reduces the standard error bars of the fitted parameters with a least square minimization method (*i.e.* the root mean square of diagonal elements of the covariance matrix). Figures 5c,d show the Arrhenius plots including experimental data and the fitting curves considering separately the P_a and P_b decays from the eq 2. The P_a decay describes the evolution of experimental data at low temperature, whereas the P_b decay is associated with the high temperature behavior.

The result of the analysis of temperature-dependent PL experiments for all the samples is presented in Figure 6. Figure 6a shows the ratio of the QW peak intensities measured at 300 and 10 K ($I_{300\text{ K}}/I_{10\text{ K}}$) as a function of QW thickness. Assuming that recombination at low temperature is only radiative, $I_{300\text{ K}}/I_{10\text{ K}}$ corresponds to the IQE under low injection conditions ($\approx 10\text{ W/cm}^2$).^{44,45} As shown in Figure 6a, the maximum value is IQE = 7.3%, obtained for 2.6-nm-thick QWs emitting at 325 nm. By decreasing the QW thickness, $I_{300\text{ K}}/I_{10\text{ K}}$ decreases to 1.7% for the thinnest QW sample emitting at 292 nm. On the other hand, for QW thicknesses larger than 2.6 nm, the ratio suddenly drops to

values as low as 0.15% for the thicker QW sample. To try to understand this behavior, we have analyzed the evolution of the parameters of eq 2 (activation energies and weighting prefactors) as a function of the QW thickness. The results are summarized in Figures 6b,c and Table S9. The lower activation energy $E_a = 15 \pm 9$ meV (the error bar corresponds to the standard deviation) remains approximately constant with the QW thickness. On the contrary, E_b increases from ≈ 100 meV for QW thicknesses ≤ 2.6 nm to values close to 200 meV for the thicker samples (3.3 and 4.3 nm). Unfortunately, the increase of E_b , which should lead to an increase of the IQE, is compensated by a drastic increase of the weight prefactor b in these two samples. Note that the activation energy is the potential barrier that separates carriers from non-radiative recombination centers, and the prefactors are related to the radiative vs. non-radiative recombination time.⁴³ Therefore, the effect of higher activation energy can be compensated if the non-radiative recombination time is faster.

To visualize the dominant non-radiative process, the evolution of ratio $P_b/P_a = (b/a) \exp[(-E_b + E_a)/k_B T]$ is plotted in Figure 6d as a function of the QW thickness at different temperatures (130, 160, 200 and 300 K). When the P_b/P_a ratio is equal to 1, the number of non-radiative recombination is the same for the two processes. This transition, indicated by the vertical green lines in Figures 5c,d and in Figure 6d, occurs in the range of 120-170 K. Above $T = 200$ K, the P_b process mainly controls the emission decay especially for the two thickest QW samples (3.3 and 4.3 nm), in agreement with the evolution of the parameters shown in Figures 6c,d.

Bi-exponential decay of the PL intensity with temperature has been previously observed in III-nitrides. For instance, a study of Al-rich AlGa_N films has reported similar temperature quenching with two activation energies $E_1 \sim 10$ meV and $E_2 \sim 130$ meV, which were assigned to non-identified point defects and negatively-charged V_{Al-O_N}

complexes, respectively.⁴⁶ Another study of MBE [0001]-oriented GaN/AlGaN QWs also reported double activation energies with $E_1 = 15 \pm 3$ meV and $E_2 = 110 \pm 15$ meV. In this case, the higher activation energy was tentatively attributed to carrier localization induced by structural defects or QW thickness fluctuations.⁴⁷ In the case of nanowires, a recent study of GaAs/GaNAs/GaAs core-shell heterostructures showed a bi-exponential decay of the PL intensity with temperature, with $E_1 = 12$ meV and $E_2 = 63$ meV, probably associated with the presence of gallium interstitials and vacancies.⁴⁸ In our study, the non-radiative path activated at low temperature seems to be an intrinsic phenomenon, which shows no correlation with the QW thickness (Figures 6b,c). On the contrary, the non-radiative process dominant at high temperature (P_b) can be directly correlated with the drop of the $I_{300\text{ K}}/I_{10\text{ K}}$ ratio observed in Figure 6a. Further advanced optical and structural characterizations are required to identify the physical origin of this non-radiative recombination path.

■ CONCLUSIONS

In conclusion, this paper reports a detailed analysis of the optical and structural properties of *m*-plane core-shell GaN/AlGaN MQWs grown on catalyst-free and silane assisted \bar{c} -GaN microwires by MOVPE. We have studied the effect of decreasing the GaN QW thicknesses from 4.3 to 0.7 nm in MQWs with ~ 5.5 nm-thick AlGaN barriers. HRTEM images reveal heterostructures with high crystalline quality and sharp interfaces. The QW emission along the non-polar *m*-plane wire sidewalls is demonstrated. The reduction of the QW thickness induces a blue shift of the luminescence down to 292 nm for the thinnest QWs (0.7 nm). These observations show excellent agreement with 8-band $\mathbf{k}\cdot\mathbf{p}$ Schrödinger-Poisson calculations assuming $\sim 60\%$ Al-content in the barriers.

Temperature-dependent PL studies performed under low injection conditions (10 W/cm^2) showed an S-shape spectral evolution of the luminescence, which is assigned to carrier localization presumably due to GaN thickness fluctuations. Localization is more important in thinner QWs. The IQE evaluated from the PL intensity ratio between 300 K and 10 K is maximum for 2.6-nm-thick QWs (7.3%) emitting at 325 nm. We demonstrate that the evolution of the QW emission intensity as a function of temperature is well described by considering two non-radiative recombination paths with different activation energies, namely $E_a = 15 \pm 9 \text{ meV}$, approximately independent of the QW thickness, and E_b , which increases from $\approx 100 \text{ meV}$ for QW thicknesses $\leq 2.6 \text{ nm}$ to values close to 200 meV for the thicker samples (3.3 and 4.3 nm). We conclude that the low temperature path is intrinsic to the GaN materials, whereas the high temperature process is associated with the drop of the internal quantum efficiency. This understanding constitutes a step forward to the fabrication by MOVPE of wire-based devices emitting in the UV-A,B domains.

■ ASSOCIATED CONTENT

Supporting Information

The Supporting Information is available free of charge at [XXX](#).

STEM-HAADF observations along the wire length; Nextnano³ calculations estimating the influence of the QW thickness variation on the emission energy; PL emission energy for thin QW samples; evidences of carrier localization for thin QW samples from CL mappings; details about the fit of PL intensity as a function of temperature ([PDF](#))

■ AUTHOR INFORMATION

Corresponding authors

*Vincent Grenier - *Univ. Grenoble Alpes, CEA, IRIG, PHELIQS, NPSC, 38000 Grenoble, France*; Email: vincent.grenier@cea.fr

*Christophe Durand - *Univ. Grenoble Alpes, CEA, IRIG, PHELIQS, NPSC, 38000 Grenoble, France*; orcid.org/0000-0002-5012-8411;
Email: christophe.durand@cea.fr

Authors

Sylvain Finot - *Univ. Grenoble Alpes, CNRS, Institut Néel, 38000 Grenoble, France*;
Email: sylvain.finot@neel.cnrs.fr

Gwénoél Jacopin - *Univ. Grenoble Alpes, CNRS, Institut Néel, 38000 Grenoble, France*; orcid.org/0000-0003-0049-7195;
Email: gwenole.jacopin@neel.cnrs.fr

Catherine Bougerol - *Univ. Grenoble Alpes, CNRS, Institut Néel, 38000 Grenoble, France*; orcid.org/0000-0002-4823-0919;
Email: catherine.bougerol@neel.cnrs.fr

Nicolas Mollard - *Univ. Grenoble Alpes, CEA, IRIG, PHELIQS, NPSC, 38000 Grenoble, France*; Email: nicolas.mollard@cea.fr

Bruno Gayral - *Univ. Grenoble Alpes, CEA, IRIG, PHELIQS, NPSC, 38000 Grenoble, France*; Email: bruno.gayral@cea.fr

Eva Monroy - *Univ. Grenoble Alpes, CEA, IRIG, PHELIQS, NPSC, 38000 Grenoble, France*; orcid.org/0000-0001-5481-3267; Email: eva.monroy@cea.fr

Joël Eymery - *Univ. Grenoble Alpes, CEA, IRG, MEM, NRS, 38000 Grenoble, France*; orcid.org/0000-0002-4216-1166; Email: joel.eymery@cea.fr

Author Contributions

V.G. made the wire growth and took an active part in the writing of this manuscript with support from the supervisors C.D. and J.E. who designed the study. S.F and G.J performed the cathodoluminescence measurements and data treatments. C.B. performed the STEM/TEM measurements. The FIB preparation, photoluminescence measurements and nextnano³ calculations were performed by V.G. thanks to the trainings of N.M., B.G. and E.M. respectively. All authors contributed to the discussions and have given approval to the final version of the manuscript.

Notes

The authors declare no competing financial interest.

■ ACKNOWLEDGMENTS

This work has been financially supported by the program “Initiatives de Recherche Stratégiques » (IRS) of IDEX Univ. Grenoble Alpes (15-IDEX-0002) and by the French-Irish program ULYSSES administered by the Irish Research Council and Campus-France.

The authors would like to thank J. Dussaud for his work on the MOVPE setup and N. Mollard for his support in FIB preparation.

Figure Caption:

Figure 1. (a) 30°-tilted SEM image of an assembly of \bar{c} -oriented GaN wires grown on c-sapphire substrate. (b) SEM image of a single core-shell GaN wire dispersed on a Si substrate. Images (a) and (b) are obtained with 3 kV electron beam acceleration voltage. (c) Schematic of GaN wire showing the different doping regions and the m -plane GaN/AlGaN MQWs core-shell heterostructure.

Figure 2. Images of longitudinal cross sections of GaN/AlGaN core-shell wires with ten GaN QWs of 4.3 nm (a-c) and 2.6 nm (d-f) thickness: HAADF-STEM images (a,b,d,e) at different magnifications and off-axis HR-TEM images (c, f) with 10° tilt from the $[11\bar{2}0]$ zone axis along $[10\bar{1}0]$.

Figure 3. (a,c) SEM images of typical single wires of samples with 4.3 and 2.6 nm GaN QWs and (b,d) corresponding CL studies performed at 5 K. (b,d) Left: CL spectra as a function of the wire length. Right: CL map of the emission integrated over the FWHM of the QW signal (range indicated in the figure).

Figure 4. (a) Normalized-intensity PL spectra of GaN/AlGaN core-shell wires with QW thickness varying from 4.3 to 0.7 nm, measured at 10 K from an assembly of wires dispersed on silicon using a laser at 244 nm wavelength and an excitation power ~ 10 W/cm². (b) Red dots represent the emission energy of the samples shown in Figure 4a,

as a function of the QW thickness. The error bars indicate the dispersion after 3-5 measurements on different locations of the sample under the same excitation conditions. The experimental data are compared with 1D nextnano³ calculations of the band-to-band transition energy e_1-h_1 for 5x(GaN/5.5 nm Al_{0.6}Ga_{0.4}N) MQWs, assumed fully strained on GaN (blue line plus symbols), Al_{0.6}Ga_{0.4}N (dark line plus symbols) and on Al \bar{x} Ga_(1- \bar{x})N, with \bar{x} being the average Al mole fraction of the MQW (green line plus symbols).

Figure 5. (a), (b) Temperature-dependent PL spectra of GaN/AlGaN core-shell wires with 4.3 and 2.6 nm GaN QWs. The inset shows the QW peak emission energy as a function of temperature. (c),(d) Normalized Arrhenius plot of the maximum PL intensity of GaN/AlGaN core-shell wires with 4.3 and 2.6 nm-thick GaN QWs. Blue dots are experimental data and dashed lines represent the evolution resulting from each non-radiative recombination paths, obtained by fitting the experimental data using eq 2. The processes with low (high) activation energy P_a (P_b) are drawn in yellow (red). The $P_a = P_b$ point is depicted with a vertical green line.

Figure 6. (a) PL intensity ratio between 300 and 10 K as a function of the QW thickness. (b) Variation as a function of the QW thickness of: (b) the weighting factors a and b , (c) the two activation energies E_a and E_b corresponding to the non-radiative recombination processes described by P_a and P_b . (d) Variation of the P_b/P_a ratio as a function of the QW thickness at different temperatures (130, 160, 200, and 300 K). The ratio equal to 1 is marked with a horizontal green line.

Figure 1

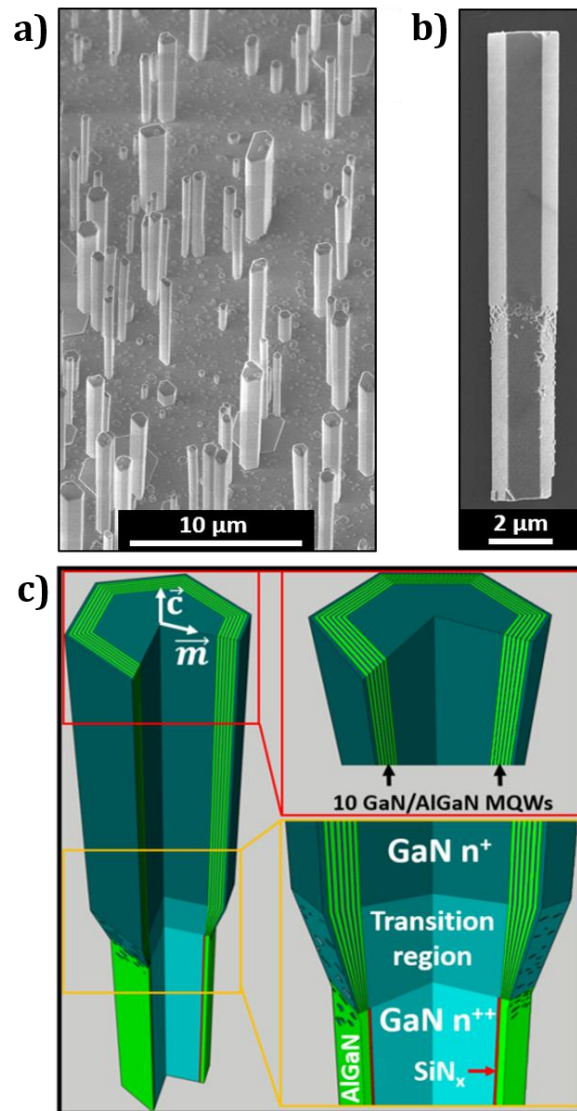


Figure 2

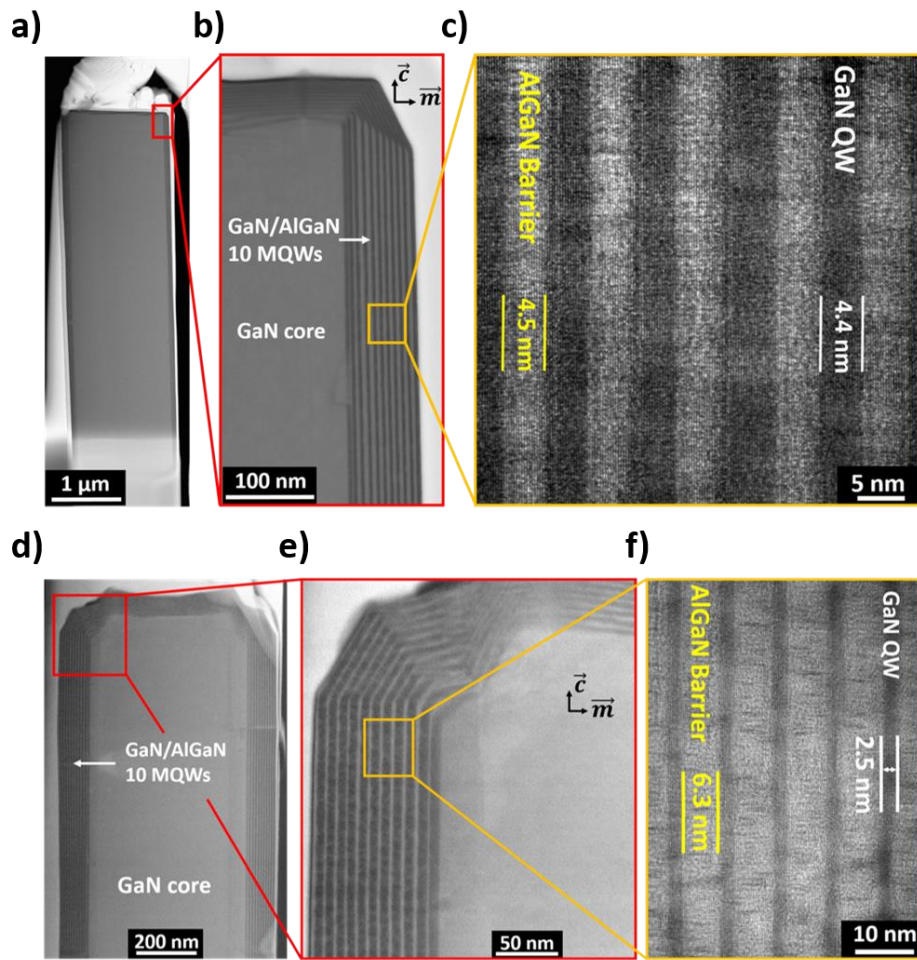


Figure 3

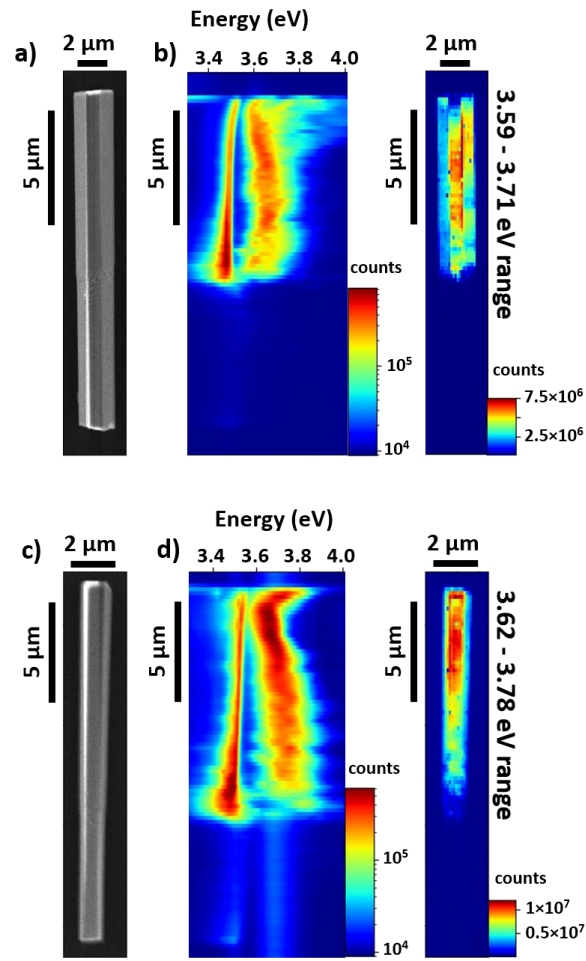


Figure 4

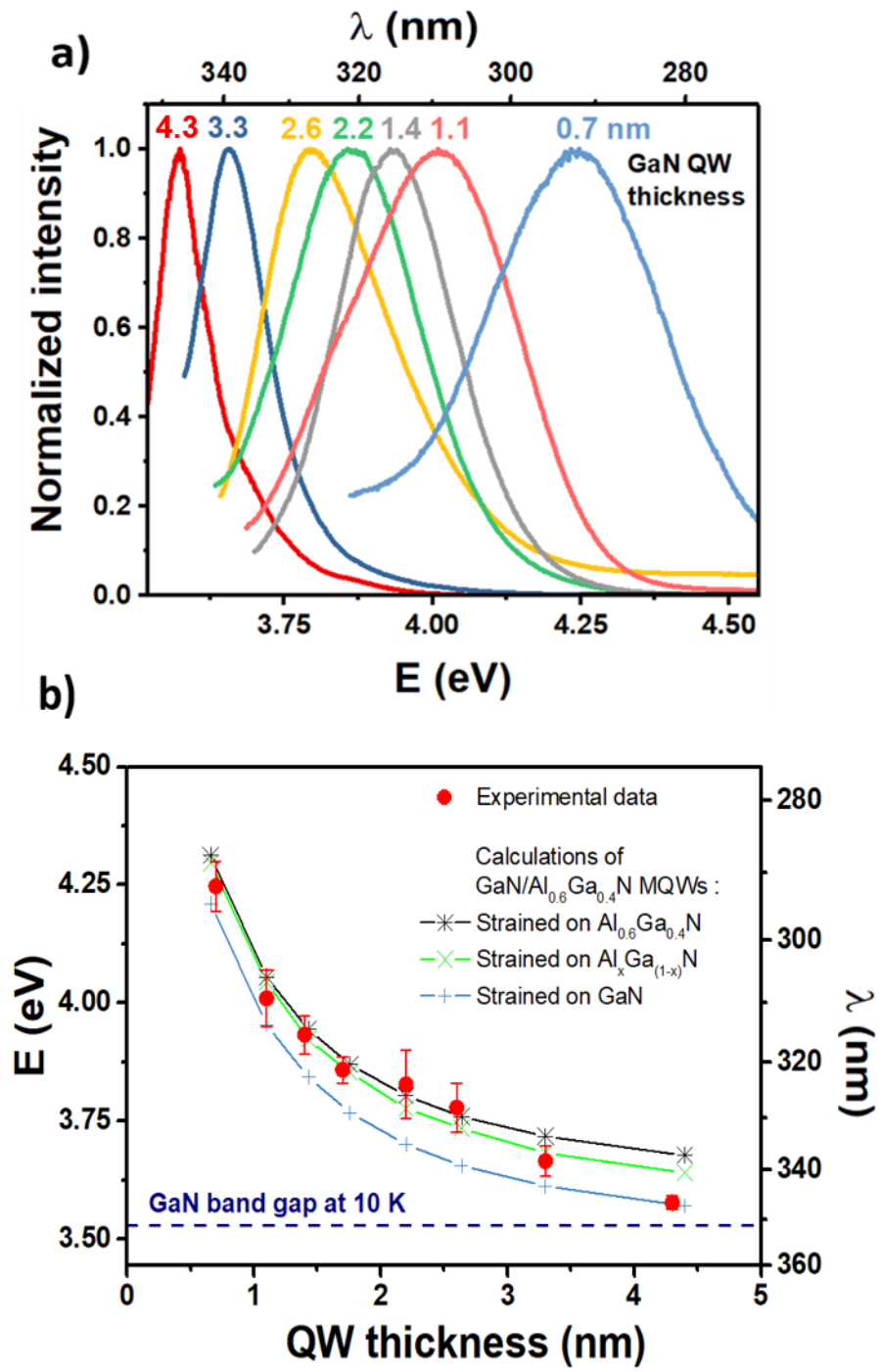


Figure 5

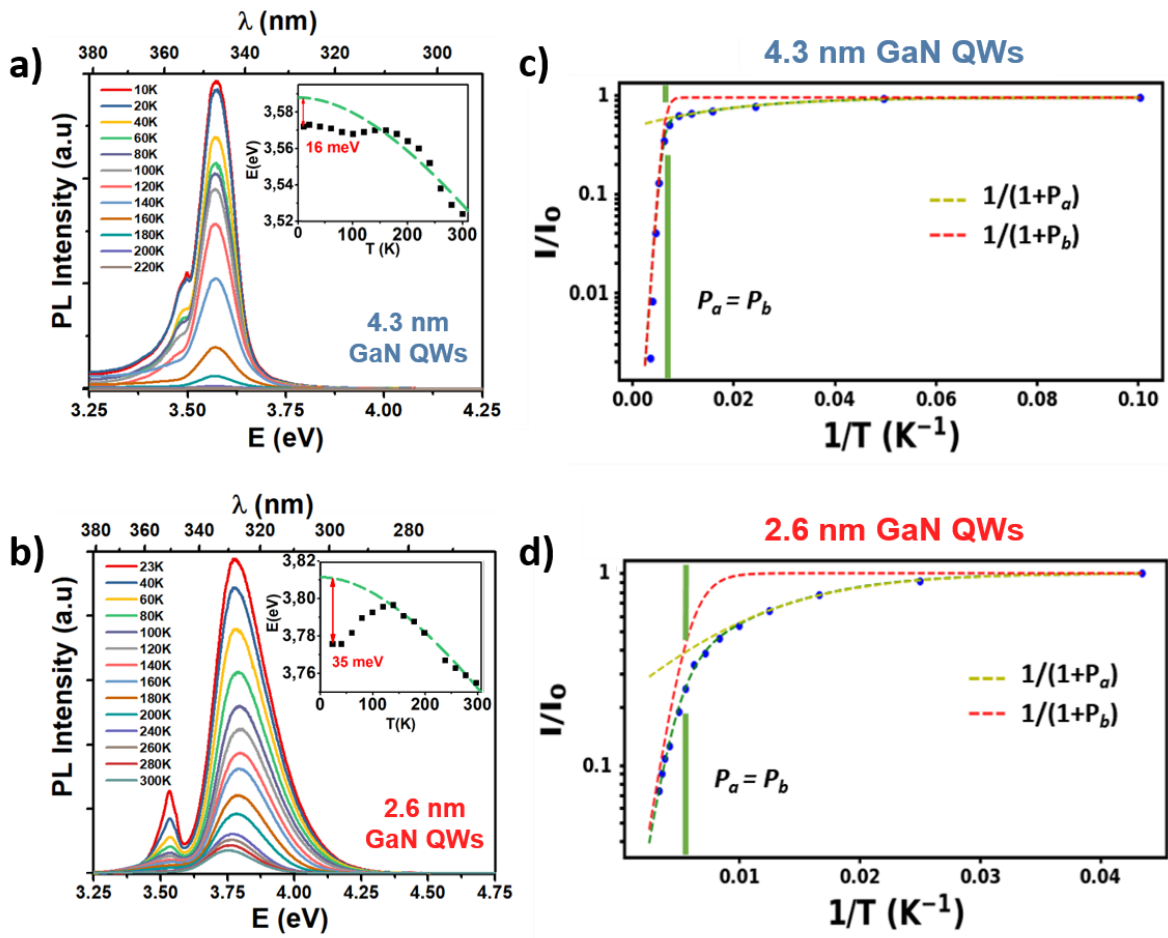
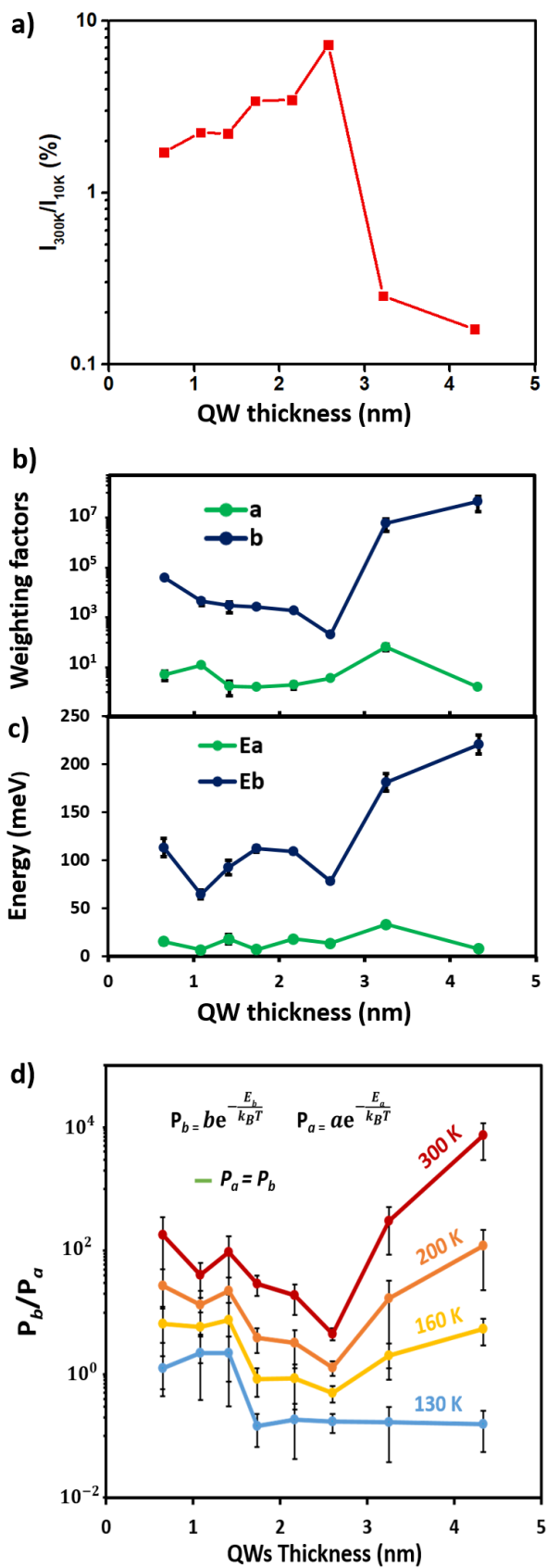


Figure 6



■ REFERENCES

- (1) Shur, M.; Shatalov, M.; Dobrinsky, A.; Gaska, R. Deep Ultraviolet Light-Emitting Diodes. *Springer Series in Materials Science*. 2012, pp 83–120.
https://doi.org/10.1007/978-3-642-23521-4_3.
- (2) Kneissl, M.; Seong, T. Y.; Han, J.; Amano, H. The Emergence and Prospects of Deep-Ultraviolet Light-Emitting Diode Technologies. *Nature Photonics*. Nature Publishing Group April 1, 2019, pp 233–244. <https://doi.org/10.1038/s41566-019-0359-9>.
- (3) Connie, A. T.; Zhao, S.; Sadaf, S. M.; Shih, I.; Mi, Z.; Du, X.; Lin, J.; Jiang, H. Optical and Electrical Properties of Mg-Doped AlN Nanowires Grown by Molecular Beam Epitaxy. *Appl. Phys. Lett.* **2015**, *106* (21). <https://doi.org/10.1063/1.4921626>.
- (4) Tran, N. H.; Le, B. H.; Zhao, S.; Mi, Z. On the Mechanism of Highly Efficient P-Type Conduction of Mg-Doped Ultra-Wide-Bandgap AlN Nanostructures. *Appl. Phys. Lett.* **2017**, *110* (3). <https://doi.org/10.1063/1.4973999>.
- (5) Siladie, A. M.; Jacopin, G.; Cros, A.; Garro, N.; Robin, E.; Caliste, D.; Pochet, P.; Donatini, F.; Pernot, J.; Daudin, B. Mg and in Codoped P-Type AlN Nanowires for Pn Junction Realization. *Nano Lett.* **2019**, *19* (12), 8357–8364.
<https://doi.org/10.1021/acs.nanolett.9b01394>.
- (6) Laleyan, D. A.; Zhao, S.; Woo, S. Y.; Tran, H. N.; Le, H. B.; Szkopek, T.; Guo, H.; Botton, G. A.; Mi, Z. AlN/h-BN Heterostructures for Mg Dopant-Free Deep Ultraviolet Photonics. *Nano Lett.* **2017**, *17* (6), 3738–3743.
<https://doi.org/10.1021/acs.nanolett.7b01068>.
- (7) Zhang, L.; Guo, Y.; Yan, J.; Wu, Q.; Lu, Y.; Wu, Z.; Gu, W.; Wei, X.; Wang, J.; Li, J. Deep

- Ultraviolet Light-Emitting Diodes Based on a Well-Ordered AlGa_N Nanorod Array. *Photonics Res.* **2019**, *7* (9), B66. <https://doi.org/10.1364/prj.7.000b66>.
- (8) Zhao; Lu; Hai; Yin. AlGa_N Nanowires for Ultraviolet Light-Emitting: Recent Progress, Challenges, and Prospects. *Micromachines* **2020**, *11* (2), 125. <https://doi.org/10.3390/mi11020125>.
- (9) Dimkou, I.; Harikumar, A.; Donatini, F.; Lähnemann, J.; Den Hertog, M. I.; Bougerol, C.; Bellet-Amalric, E.; Mollard, N.; Ajay, A.; Ledoux, G.; et al. Assessment of AlGa_N/Al_N Superlattices on Ga_N Nanowires as Active Region of Electron-Pumped Ultraviolet Sources. *Nanotechnology* **2020**, *31* (20). <https://doi.org/10.1088/1361-6528/ab704d>.
- (10) Coulon, P. M.; Kusch, G.; Le Boulbar, E. D.; Chausse, P.; Bryce, C.; Martin, R. W.; Shields, P. A. Hybrid Top-Down/Bottom-Up Fabrication of Regular Arrays of Al_N Nanorods for Deep-UV Core–Shell LEDs. *Phys. Status Solidi Basic Res.* **2018**, *255* (5). <https://doi.org/10.1002/pssb.201700445>.
- (11) Coulon, P. M.; Kusch, G.; Martin, R. W.; Shields, P. A. Deep UV Emission from Highly Ordered AlGa_N/Al_N Core-Shell Nanorods. *ACS Appl. Mater. Interfaces* **2018**, *10* (39), 33441–33449. <https://doi.org/10.1021/acsami.8b10605>.
- (12) Conroy, M.; Zubialeovich, V. Z.; Li, H.; Petkov, N.; O'Donoghue, S.; Holmes, J. D.; Parbrook, P. J. Ultra-High-Density Arrays of Defect-Free Al_N Nanorods: A 'Space-Filling' Approach. *ACS Nano* **2016**, *10* (2), 1988–1994. <https://doi.org/10.1021/acsnano.5b06062>.
- (13) Kang, S.; Chatterjee, U.; Um, D. Y.; Yu, Y. T.; Seo, I. S.; Lee, C. R. Ultraviolet-C Photodetector Fabricated Using Si-Doped n-AlGa_N Nanorods Grown by MOCVD. *ACS Photonics* **2017**, *4* (10), 2595–2603. <https://doi.org/10.1021/acsp Photonics.7b01047>.

- (14) Ren, F.; Yin, Y.; Wang, Y.; Liu, Z.; Liang, M.; Ou, H.; Ao, J.; Wei, T.; Yan, J.; Yuan, G.; et al. Direct Growth Of AlGa_N Nanorod LEDs on Graphene-Covered Si. *Materials (Basel)*. **2018**, *11* (12). <https://doi.org/10.3390/ma11122372>.
- (15) Durand, C.; Bougerol, C.; Carlin, J. F.; Rossbach, G.; Godel, F.; Eymery, J.; Jouneau, P. H.; Mukhtarova, A.; Butté, R.; Grandjean, N. M-Plane GaN/InAlN Multiple Quantum Wells in Core-Shell Wire Structure for UV Emission. *ACS Photonics* **2014**, *1* (1), 38–46. <https://doi.org/10.1021/ph400031x>.
- (16) Brubaker, M. D.; Genter, K. L.; Roshko, A.; Blanchard, P. T.; Spann, B. T.; Harvey, T. E.; Bertness, K. A. UV LEDs Based on P-i-n Core-Shell AlGa_N/Ga_N Nanowire Heterostructures Grown by N-Polar Selective Area Epitaxy. *Nanotechnology* **2019**, *30* (23). <https://doi.org/10.1088/1361-6528/ab07ed>.
- (17) Ra, Y. H.; Kang, S.; Lee, C. R. Ultraviolet Light-Emitting Diode Using Nonpolar AlGa_N Core–Shell Nanowire Heterostructures. *Adv. Opt. Mater.* **2018**, *6* (14). <https://doi.org/10.1002/adom.201701391>.
- (18) Koester, R.; Hwang, J. S.; Salomon, D.; Chen, X.; Bougerol, C.; Barnes, J. P.; Dang, D. L. S.; Rigutti, L.; De Luna Bugallo, A.; Jacopin, G.; et al. M-Plane Core-Shell InGa_N/Ga_N Multiple-Quantum-Wells on Ga_N Wires for Electroluminescent Devices. *Nano Lett.* **2011**, *11* (11), 4839–4845. <https://doi.org/10.1021/nl202686n>.
- (19) Kapoor, A.; Guan, N.; Vallo, M.; Messanvi, A.; Mancini, L.; Gautier, E.; Bougerol, C.; Gayral, B.; Julien, F. H.; Vurpillot, F.; et al. Green Electroluminescence from Radial M-Plane InGa_N Quantum Wells Grown on Ga_N Wire Sidewalls by Metal-Organic Vapor Phase Epitaxy. *ACS Photonics* **2018**, *5* (11), 4330–4337. <https://doi.org/10.1021/acsp Photonics.8b00520>.
- (20) Dai, X.; Messanvi, A.; Zhang, H.; Durand, C.; Eymery, J.; Bougerol, C.; Julien, F. H.;

- Tchernycheva, M. Flexible Light-Emitting Diodes Based on Vertical Nitride Nanowires. *Nano Lett.* **2015**, *15*, 6958–6964.
<https://doi.org/10.1021/acs.nanolett.5b02900>.
- (21) Kim, J.; Choi, U.; Pyeon, J.; So, B.; Nam, O. Deep-Ultraviolet AlGaN/AlN Core-Shell Multiple Quantum Wells on AlN Nanorods via Lithography-Free Method. *Sci. Rep.* **2018**, *8* (1). <https://doi.org/10.1038/s41598-017-19047-6>.
- (22) Durand, C.; Carlin, J. F.; Bougerol, C.; Gayral, B.; Salomon, D.; Barnes, J. P.; Eymery, J.; Butté, R.; Grandjean, N. Thin-Wall GaN/InAlN Multiple Quantum Well Tubes. *Nano Lett.* **2017**. <https://doi.org/10.1021/acs.nanolett.6b04852>.
- (23) Koester, R.; Hwang, J. S.; Durand, C.; Le Si Dang, D.; Eymery, J. Self-Assembled Growth of Catalyst-Free GaN Wires by Metal-Organic Vapour Phase Epitaxy. *Nanotechnology* **2010**, *21* (1). <https://doi.org/10.1088/0957-4484/21/1/015602>.
- (24) Tchoufian, P.; Donatini, F.; Levy, F.; Amstatt, B.; Ferret, P.; Pernot, J. High Conductivity in Si-Doped GaN Wires. *Appl. Phys. Lett.* **2013**, *102* (12).
<https://doi.org/10.1063/1.4799167>.
- (25) Tchoufian, P.; Donatini, F.; Levy, F.; Dussaigne, A.; Ferret, P.; Pernot, J. Direct Imaging of P-n Junction in Core-Shell GaN Wires. *Nano Lett.* **2014**, *14* (6), 3491–3498. <https://doi.org/10.1021/nl5010493>.
- (26) Kapoor, A.; Finot, S.; Grenier, V.; Robin, E.; Bougerol, C.; Bleuse, J.; Jacopin, G.; Eymery, J.; Durand, C. Role of Underlayer for Efficient Core-Shell InGaN QWs Grown on m-Plane GaN Wire Sidewalls. *ACS Appl. Mater. Interfaces* **2020**.
<https://doi.org/https://doi.org/10.1021/acsami.9b19314>.
- (27) Gilet, P.; Dussaigne, A.; Salomon, D.; Eymery, J.; Durand, C. Optoelectronic Device Comprising Three-Dimensional Semiconductors Elements, and Method for

- Manufacturing Said Device. US Pat. App.15/745,429, July 26, 2018.
- (28) Chen, X. J.; Perillat-Merceroz, G.; Sam-Giao, D.; Durand, C.; Eymery, J.
Homoepitaxial Growth of Catalyst-Free GaN Wires on N-Polar Substrates. *Appl. Phys. Lett.* **2010**, *97* (15). <https://doi.org/10.1063/1.3497078>.
- (29) Eymery, J.; Salomon, D.; Chen, X.; Durand, C. Process for Catalyst-Free Selective Growth on a Semiconductor Structure. Pat. WO/2012/136665, 2012.
- (30) Koester, R.; Hwang, J. S.; Salomon, D.; Chen, X.; Bougerol, C.; Barnes, J. P.; Dang, D. L. S.; Rigutti, L.; De Luna Bugallo, A.; Jacopin, G.; et al. M-Plane Core-Shell InGaN/GaN Multiple-Quantum-Wells on GaN Wires for Electroluminescent Devices. *Nano Lett.* **2011**. <https://doi.org/10.1021/nl202686n>.
- (31) Tessarek, C.; Rechberger, S.; Dieker, C.; Heilmann, M.; Spiecker, E.; Christiansen, S. Understanding GaN/InGaN Core-Shell Growth towards High Quality Factor Whispering Gallery Modes from Non-Polar InGaN Quantum Wells on GaN Rods. *Nanotechnology* **2017**, *28* (48). <https://doi.org/10.1088/1361-6528/aa9050>.
- (32) Vashaei, Z.; Bayram, C.; Lavenus, P.; Razeghi, M. Photoluminescence Characteristics of Polar and Nonpolar AlGaIn/GaN Superlattices. *Appl. Phys. Lett.* **2010**, *97* (12). <https://doi.org/10.1063/1.3493185>.
- (33) Birner, S.; Hackenbuchner, S.; Sabathil, M.; Zandler, G.; Majewski, J. A.; Andlauer, T.; Zibold, T.; Morschl, R.; Trellakis, A.; Vogl, P. Modeling of Semiconductor Nanostructures with Nextnano3. *Acta Phys. Pol. A* **2006**. <https://doi.org/10.12693/APhysPolA.110.111>.
- (34) Kandaswamy, P. K.; Guillot, F.; Bellet-Amalric, E.; Monroy, E.; Nevou, L.; Tchernycheva, M.; Michon, A.; Julien, F. H.; Baumann, E.; Giorgetta, F. R.; et al. GaN/AlN Short-Period Superlattices for Intersubband Optoelectronics: A Systematic Study of Their Epitaxial Growth, Design, and Performance. *J. Appl. Phys.*

- 2008**, *104* (9). <https://doi.org/10.1063/1.3003507>.
- (35) Leroux, M.; Beaumont, B.; Grandjean, N.; Lorenzini, P.; Haffouz, S.; Vennéguès, P.; Massies, J.; Gibart, P. Luminescence and Reflectivity Studies of Undoped, n- And p-Doped GaN on (0001) Sapphire. *Mater. Sci. Eng. B* **1997**, *50* (1–3), 97–104. [https://doi.org/10.1016/S0921-5107\(97\)00143-8](https://doi.org/10.1016/S0921-5107(97)00143-8).
- (36) Monemar, B. *Bound Excitons in GaN*; 2001; Vol. 13.
- (37) Calle, F.; Sánchez, F. J.; Tijero, J. M. G.; Sánchez-García, M. A.; Calleja, E.; Beresford, R. Exciton and Donor-Acceptor Recombination in Undoped GaN on Si(111). *Semicond. Sci. Technol.* **1997**, *12* (11), 1396–1403. <https://doi.org/10.1088/0268-1242/12/11/011>.
- (38) Feneberg, M.; Osterburg, S.; Lange, K.; Lidig, C.; Garke, B.; Goldhahn, R.; Richter, E.; Netzel, C.; Neumann, M. D.; Esser, N.; et al. Band Gap Renormalization and Burstein-Moss Effect in Silicon- and Germanium-Doped Wurtzite GaN up to 1020 Cm-3. *Phys. Rev. B - Condens. Matter Mater. Phys.* **2014**, *90* (7). <https://doi.org/10.1103/PhysRevB.90.075203>.
- (39) Sasaki, A.; Nishizuka, K.; Wang, T.; Sakai, S.; Kaneta, A.; Kawakami, Y.; Fujita, S. Radiative Carrier Recombination Dependent on Temperature and Well Width of InGaN/GaN Single Quantum Well. *Solid State Commun.* **2004**, *129* (1), 31–35. <https://doi.org/10.1016/j.ssc.2003.09.018>.
- (40) Lefebvre, P.; Taliercio, T.; Morel, A.; Allègre, J.; Gallart, M.; Gil, B.; Mathieu, H.; Damilano, B.; Grandjean, N.; Massies, J. Effects of GaAlN Barriers and of Dimensionality on Optical Recombination Processes in InGaN Quantum Wells and Quantum Boxes. *Appl. Phys. Lett.* **2001**, *78* (11), 1538–1540. <https://doi.org/10.1063/1.1352664>.
- (41) Rigutti, L.; Mancini, L.; Lefebvre, W.; Houard, J.; Hernández-Maldonado, D.; Di

- Russo, E.; Giraud, E.; Butté, R.; Carlin, J. F.; Grandjean, N.; et al. Statistical Nanoscale Study of Localised Radiative Transitions in GaN/AlGa_N Quantum Wells and AlGa_N Epitaxial Layers. *Semicond. Sci. Technol.* **2016**, *31* (9).
<https://doi.org/10.1088/0268-1242/31/9/095009>.
- (42) Li, Y.; Lu, Y.; Shen, H.; Wraback, M.; Brown, M. G.; Schurman, M.; Koszi, L.; Stall, R. A. Temperature Dependence of Energy Gap in GaN Thin Film Studied by Thermomodulation. *Appl. Phys. Lett.* **1997**, *70* (18), 2458–2460.
<https://doi.org/10.1063/1.118855>.
- (43) Leroux, M.; Grandjean, N.; Beaumont, B.; Nataf, G.; Semond, F.; Massies, J.; Gibart, P. Temperature Quenching of Photoluminescence Intensities in Undoped and Doped GaN. *J. Appl. Phys.* **1999**, *86* (7), 3721–3728. <https://doi.org/10.1063/1.371242>.
- (44) Watanabe, S.; Yamada, N.; Nagashima, M.; Ueki, Y.; Sasaki, C.; Yamada, Y.; Taguchi, T.; Tadatomo, K.; Okagawa, H.; Kudo, H. Internal Quantum Efficiency of Highly-Efficient In(x)Ga(1-x)N-Based near-Ultraviolet Light-Emitting Diodes. *Appl. Phys. Lett.* **2003**, *83* (24), 4906–4908. <https://doi.org/10.1063/1.1633672>.
- (45) Murotani, H.; Yamada, Y.; Tabata, T.; Honda, Y.; Yamaguchi, M.; Amano, H. Effects of Exciton Localization on Internal Quantum Efficiency of InGa_N Nanowires. *J. Appl. Phys.* **2013**, *114* (15). <https://doi.org/10.1063/1.4825124>.
- (46) Ichikawa, S.; Funato, M.; Kawakami, Y. Dominant Nonradiative Recombination Paths and Their Activation Processes in Al_xGa_{1-x}N -Related Materials. *Phys. Rev. Appl.* **2018**, *10* (6). <https://doi.org/10.1103/PhysRevApplied.10.064027>.
- (47) Gačević, Ž.; Das, A.; Teubert, J.; Kotsar, Y.; Kandaswamy, P. K.; Kehagias, T.; Koukoulas, T.; Komninou, P.; Monroy, E. Internal Quantum Efficiency of III-Nitride Quantum Dot Superlattices Grown by Plasma-Assisted Molecular-Beam Epitaxy. In *Journal of Applied Physics*; 2011; Vol. 109. <https://doi.org/10.1063/1.3590151>.

- (48) Stehr, J. E.; Balagula, R. M.; Jansson, M.; Yukimune, M.; Fujiwara, R.; Ishikawa, F.; Chen, W. M.; Buyanova, I. A. Effects of Growth Temperature and Thermal Annealing on Optical Quality of GaNAs Nanowires Emitting in the Near-Infrared Spectral Range. *Nanotechnology* **2020**, *31* (6). <https://doi.org/10.1088/1361-6528/ab51cd>.